Redox Biology 12 (2017) 699–711

Contents lists available at ScienceDirect

Redox Biology

journal homepage: www.elsevier.com/locate/redox

Research Paper

Protein aggregation into insoluble deposits protects from oxidative stress

Anita Carija[a], Susanna Navarro[a], Natalia Sanchez de Groot[b,c], Salvador Ventura[a,*]

[a] Institut de Biotecnologia i Biomedicina and Departament de Bioquímica i Biologia Molecular, Universitat Autònoma de Barcelona, Bellaterra, Barcelona, Spain
[b] Centre for Genomic Regulation (CRG), The Barcelona Institute for Science and Technology, Dr. Aiguader 88, 08003 Barcelona, Spain
[c] Universitat Pompeu Fabra (UPF), Barcelona, Spain

ARTICLE INFO

Keywords:
Protein aggregation
Oxidative stress
Amyloid peptide
Protein inclusions
Yeast

ABSTRACT

Protein misfolding and aggregation have been associated with the onset of neurodegenerative disorders. Recent studies demonstrate that the aggregation process can result in a high diversity of protein conformational states, however the identity of the specific species responsible for the cellular damage is still unclear. Here, we use yeast as a model to systematically analyse the intracellular effect of expressing 21 variants of the amyloid-ß-peptide, engineered to cover a continuous range of intrinsic aggregation propensities. We demonstrate the existence of a striking negative correlation between the aggregation propensity of a given variant and the oxidative stress it elicits. Interestingly, each variant generates a specific distribution of protein assemblies in the cell. This allowed us to identify the aggregated species that remain diffusely distributed in the cytosol and are unable to coalesce into large protein inclusions as those causing the highest levels of oxidative damage. Overall, our results indicate that the formation of large insoluble aggregates may act as a protective mechanism to avoid cellular oxidative stress.

1. Introduction

Protein aggregation and the long term accumulation of amyloid protein inclusions (PI) in the central nervous system are pathognomonic signs of devastating neurodegenerative disorders like Alzheimer's (AD), Parkinson's (PD) and Huntington's (HD) diseases [1–5]. In spite of this, it is becoming evident that the coalescence of proteins and other molecules into dynamic liquid-like assemblies is essential for an increasing number of cellular processes [6–8]. In contrast, the beneficial or detrimental effects associated with the formation of insoluble protein aggregates are still under debate.

Cells have evolved two main mechanisms against protein aggregation: (i) refolding of misfolded conformers by chaperones and (ii) targeted destruction of damaged proteins by the ubiquitin-proteasome and/or autophagy systems [9–14]. The presence of PI in neurodegenerative diseases has been traditionally assumed to reflect the insufficiency of this first line of defence [15]. However, it was proposed later that the formation of PI can instead act as a protective strategy [16,17], triggering an intense dispute on the specific protein species responsible for the cellular damage [18,19]. It has been suggested that earlier aggregation intermediates, such as oligomeric and/or protofibrillar assemblies, would disrupt the cellular homeostasis by promoting aberrant interactions with different cellular components [20], including the protein quality surveillance machinery, whereas the formation of inclusions at specific cellular sites might be indeed a detoxifying mechanism against the presence of these promiscuous species [17,21]. In agreement, studies in AD, PD and HD models report that the presence of PI might represent a marker, rather than a cause of the disease and that the continuous presence of aggregative species constitutes the main toxic insult for the cell [17,22].

Oxidative stress plays a central role in the pathophysiology of the different neurodegenerative diseases linked to protein aggregation [23]. Cumulative oxidative stress induces membrane damage, impairment of the DNA repair system and mitochondrial dysfunction, which ultimately can lead to cell death [24,25]. Accordingly, there is clear evidence of oxidative damage in postmortem AD, PD and HD brains [26–28]. The mechanism by which aggregating proteins may induce oxidative stress in the brain is not completely understood, but the interaction between these two phenomena is bidirectional, in such a way that aggregation-prone conformers increase the production of reactive oxygen species (ROS), while at the same time oxidative stress exacerbates protein aggregation [28]. Again, there is discrepancy on the nature of the aggregating species causing the oxidative damage, some reports attributing this property to early oligomers [20] and

Abbreviations: ROS, reactive oxygen species; FITC, fluorescein isothiocyanate; FC, flow cytometry; PI, protein inclusion, PK, proteinase k; GFP, Green Fluorescent Protein; IP, propidium iodide

* Correspondence to: Institut de Biotecnologia i de Biomedicina, Parc de Recerca UAB, Mòdul B, Universitat Autònoma de Barcelona, E-08193 Bellaterra, Barcelona, Spain.
E-mail address: salvador.ventura@uab.es (S. Ventura).

http://dx.doi.org/10.1016/j.redox.2017.03.027
Received 21 February 2017; Accepted 6 March 2017
Available online 04 April 2017

others indicating that PI constitute centres of oxidative events, questioning their cytoprotective role [29].

The use of simple cellular models has led to great advances in the study of neurodegenerative disorders. The budding yeast *Saccharomyces cerevisiae* shares with higher eukaryotes numerous fundamental cellular pathways involved in neurodegeneration, such as protein quality control, autophagy or the regulation of the cellular redox state regulation [30,31]. Thanks to this, humanized yeast models for AD, PD and HD have been successfully developed, recapitulating some of the pathological features associated with these disorders, including oxidative stress [32–38]. We have previously exploited yeast to dissect the relationship between proteins aggregation *in vivo* and their physicochemical properties. For this purpose, we designed and expressed intracellularly 20 different variants of the amyloid-β-peptide (Aβ42) fused to GFP [39]. Later, we investigated the proteomic response caused by the expression of two individual proteins from this collection displaying different *in vivo* aggregation properties, one of them remaining diffusely distributed in the cytosol and the other one forming large PI in yeast cells. The main differences between the proteomic response elicited by these two Aβ42 variants were related to redox homeostasis [40]. This anticipated that the complete Aβ42-GFP set might be employed as a tool to dissect quantitatively the contribution of different aggregating species to oxidative damage. To this aim, in the present study we performed a systematic investigation of the relationship between the intrinsic aggregation propensities of 21 Aβ42-GFP variants, their ability to be recruited into PI and the induced intracellular oxidative stress. With these analyses, we demonstrate the existence of a conspicuous inverse relationship between Aβ42 peptides aggregation propensities and oxidative stress levels, distinguishing peptide variants unable to be recruited into inclusions as those causing the highest levels of oxidative damage. In this way, we identified as the elicitors of the oxidative insult those species that despite being in an aggregated state remain diffusely distributed in the cytosol, available for establishing disrupting non-functional interactions. Overall, our data provide strong support for the detoxifying role against oxidative stress played by PI.

2. Material and methods

2.1. Protein expression in Saccharomyces cerevisiae

Yeast cells BY4741 (MAT a *his*3Δ1 *leu*2Δ0 *met*15Δ0 *ura3*Δ0) transformed as previously described [39,41] with pESC(-Ura) plasmid (Addgene) encoding for the Aβ42-GFP protein and 19 variants differing only in the residue in position 19th of the peptide, together with the variant F19D/L34P were grown overnight in glucose SC-URA medium at 30 °C, and 100 μL was used to inoculate 5 mL of fresh medium. At an OD_{590} of 0.5, cells were changed to a fresh raffinose SC-URA medium. After 30 min of incubation, cells were changed again to a fresh SC-URA medium containing 2% of galactose, as a carbon source, to induce the recombinant protein expression during 8 h, 16 h and 48 h. Cells were harvested and pellets were stored at −80 °C.

2.2. Prediction of aggregation propensities

The aggregation propensity of the generated variants was analysed using three different algorithms: (*i*) AGGRESCAN (http://bioinf.uab.es/aggrescan/) [42], (*ii*) TANGO (http://tango.crg.es/) [43] and (*iii*) FoldAmyloid (http://bioinfo.protres.ru/fold-amyloid/) [44]. Aggregation propensities were calculated using the default settings.

2.3. Fluorescence and confocal microscopy

Cells expressing selected Aβ42-GFP variants for 8 h, 16 h and 48 h were washed with PBS and visualised by fluorescence microscopy (Nikon Eclipse TE200E). Cells were washed with PBS before image acquisition at 100-fold magnification. GFP fluorescence was acquired with a 482/35 nm laser and emission was collected at 536/40 nm. The cultures expressing Gln and Ile variants of Aβ42-GFP during 16 h, were added 10 μM dihydroethidium (Life Technologies) and incubated for 10 min in dark at 30 °C. Cells were washed in PBS, and deposited on top of glass slides. Images were obtained under UV light using a filter for GFP excitation (450–500 nm) and collecting with an emission range (515–560 nm) in a Leica fluorescence microscope (Leica Microsystems, Germany), while the fluorescence of dihydroethidium was excited using a 521–565 nm filter and the emission was collected at 553–633 nm. Image acquisition and data analysis were performed using NIS elements imaging software.

2.4. Flow cytometry analysis

Yeast cells after 8 h, 16 h and 48 h of expression were washed and resuspended in sterile PBS to an OD_{590} of 0.1. Flow cytometry measurements were performed using a BD FACSCanto flow cytometer (BD Biosciences) equipped with a 488 nm blue laser (for GFP) and 635 nm red laser (for CellROX and propidium iodide). Gated cells (by means of FSC and SSC parameters) were analysed for green emission measured on 530/30 nm BP filter and for deep red emission on 660/20 BP filter. Obtained data from 10,000 events were analysed using BD FACSDiva software (BD Biosciences) and the median fluorescence intensities at the emission maximum were obtained.

2.5. Oxidative stress detection

5 μM CellROX Deep Red Reagent (Life Technologies) was added and cells were incubated at 30 °C, for 30 min in the dark. After incubation, cells were washed 3 times and resuspended in the same volume of PBS before their analysis with flow cytometry.

2.6. Propidium iodide staining

Cell pellets were resuspended in PBS to an OD_{590} of 0.1. and incubated for 20 min with 2 μg/mL propidium iodide (here abbreviated IP to avoid confusion with protein inclusions (PI)). After incubation, cells were washed 3 times and resuspended in the same volume of PBS before their analysis with flow cytometry.

2.7. ROS assay

Hydrogen peroxide levels were determined using Red Hydrogen Peroxide Assay Kit (Enzo Life Sciences) according to manufacturer's protocol. 10 mL of cells induced for 16 h were harvested and resuspended in lysis buffer (20 mM phosphate buffer, 5 mM EDTA, 0.2 mM PMSF, pH 7.2). Cells were broken using glass beads (0.5 mm diameter) by vortexing eight times for 1 min with intervals of 1 min on ice. Supernatant was removed to new tubes and the concentration of total protein was determined by Bradford method. The conversion of red peroxidase substrate was determined by monitoring the fluorescence increase with an excitation at 531 and an emission filter at 595 nm in a Victor 3 Plate Reader (Perkin-Elmer).

2.8. Antioxidant enzyme activity determination

The catalase (CAT) activity was determined using Catalase Assay Kit (Sigma-Aldrich) according to manufacturer's protocol. 10 mL of cells expressing for 16 h were harvested, resuspended in lysis buffer (10 mM HEPES, 1.5 mM $MgCl_2$, 10 mM KCl, 0.5 mM DTT, 0.2 mM PMSF, pH 7.9) and broken as described above. The amount of remaining H_2O_2 after the action of catalase was determined by measuring the absorbance of red quinoneimine dye at 550 nm in a Victor 3 Plate Reader (Perkin-Elmer).

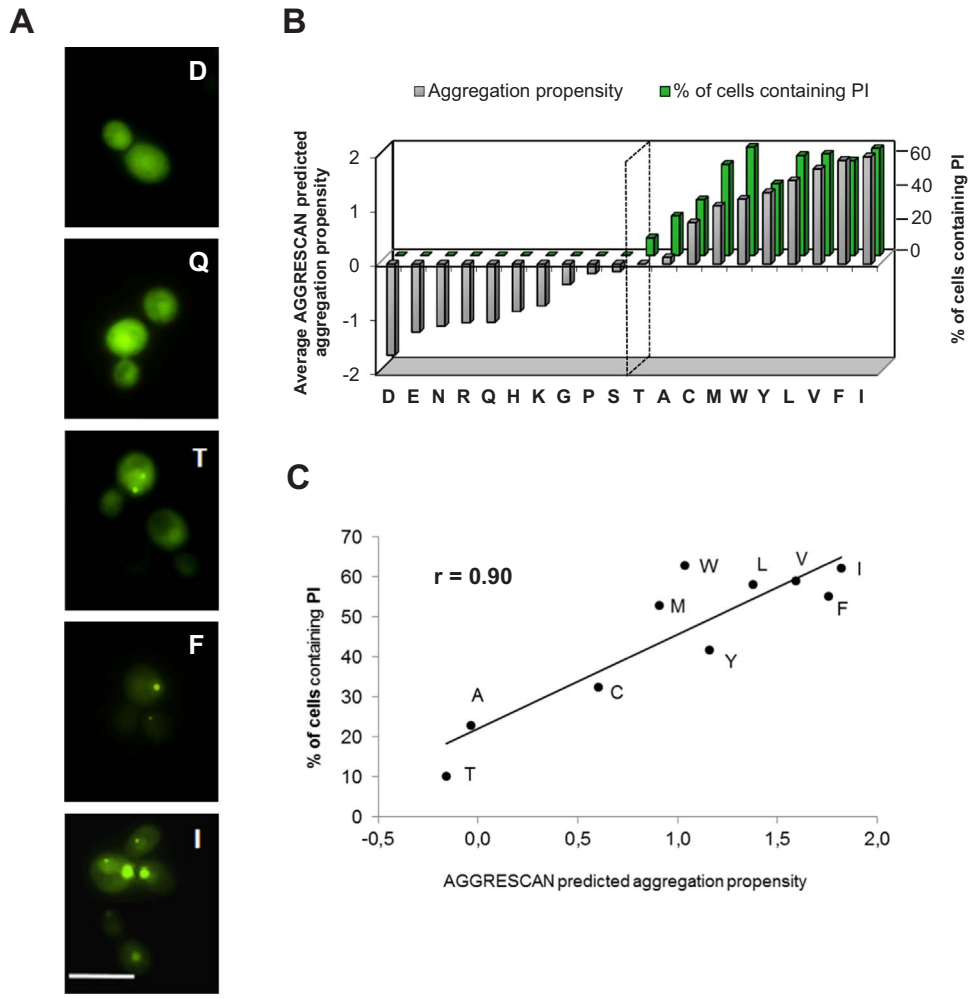

Fig. 1. GFP fluorescence determined in *S. cerevisiae* cultures expressing Aβ42-GFP mutants for 16 h. (A) Representative fluorescence microscopy images of yeast cells expressing selected Aβ42-GFP variants (Asp, Gln, Thr, Phe and Ile). Scale bar represents 10 μm. (B) 3D bar graph representing the relative aggregation propensities of 20 natural amino acids, derived from the analysis of mutants in central position of the central hydrophobic cluster in amyloid-β-protein previously described by de Groot et al. [49], represented on the primary y-axis, together with the percentage of cells containing intracellular visible fluorescent protein inclusions (PI) for Aβ42-GFP variants represented on the secondary y-axis. The dashed black line represents defined threshold of PI formation. Values were obtained by determining the number of cells with PI among the ~ 500 cells from two different cultures for each variant. (C) Correlation between the percentage of cells containing visible intracellular PI and the intrinsic aggregation propensity predicted by AGGRESCAN ($r = 0.90$, $p \leq 0.0001$).

2.9. Protein carbonylation determination

Yeast cells after 16 h of expression were broken by repeated vortexing in cold conditions using glass beads (0.6 mm diameter). Total protein extracts were centrifuged at 10,000 rpm for 10 min in order to obtain soluble fractions and at 13,000 rpm for 30 min in order to obtain insoluble fractions. Obtained fractions were boiled in 6% SDS at 90 °C for 3 min and stored at −20 °C for further analysis. Before adding SDS the concentration of the fractions was determined by Bradford method. The analysis of protein oxidation for soluble and insoluble fractions were performed by derivatization of carbonyl groups with dinitrophenylhydrazine (DNPH), followed by SDS–PAGE, transfer to PVDF membranes and western blotting, as described [45]. The antibodies employed were: anti-DNP antibody (Dako) and goat anti-rabbit IgG-HRP conjugate (Pierce). Bands were quantified by densitometry analysis using ImageLab (Bio-Rad). The level of carbonylation detected for each individual Aβ42-GFP mutant was normalised relative to the one exhibited by control cells expressing GFP alone.

2.10. Immunoblotting analysis

Collected cells were resuspended in PBS. 200 μL of each mutant was prepared to an OD_{590} of 20. For soluble/insoluble fraction analysis, 100 μL of each mutant was harvested by centrifugation and resuspended in the same volume of Y-PER protein extraction reagent (Thermo Scientific), supplemented with 1 mM PMSF, and incubated for 20 min at room temperature under mild agitation. Then the protein extract concentration was determined by Bradford method. Samples were centrifuged at maximum speed for 15 min. Soluble fractions were removed to new tubes and insoluble fractions were resuspended in 100 μL of PBS containing PMSF. 5 μL of soluble and insoluble fractions of each sample were loaded on a 15% SDS-PAGE and blotted onto a PVDF membrane. The antibodies employed were: β-amyloid antibody 6E10 (BioLegend) and goat anti-mouse IgG-HRP conjugate (Bio-Rad). Membranes were developed with Luminata (Milipore) and bands were quantified by densitometry analysis using Quantity One software (Bio-Rad).

2.11. Proteinase K resistance assay

Insoluble fractions, obtained as described above, were incubated with 10 μg/mL proteinase K (PK) (Sigma-Aldrich) in PBS at 37 °C. Aliquots digested with PK were taken at 5 and 10 min and the reaction quenched by the addition of the same amount of 4 times concentrated denaturing sample buffer. Samples were heated at 99 °C for 10 min and 5 μL of each sample was loaded on SDS-PAGE. After blotting onto a

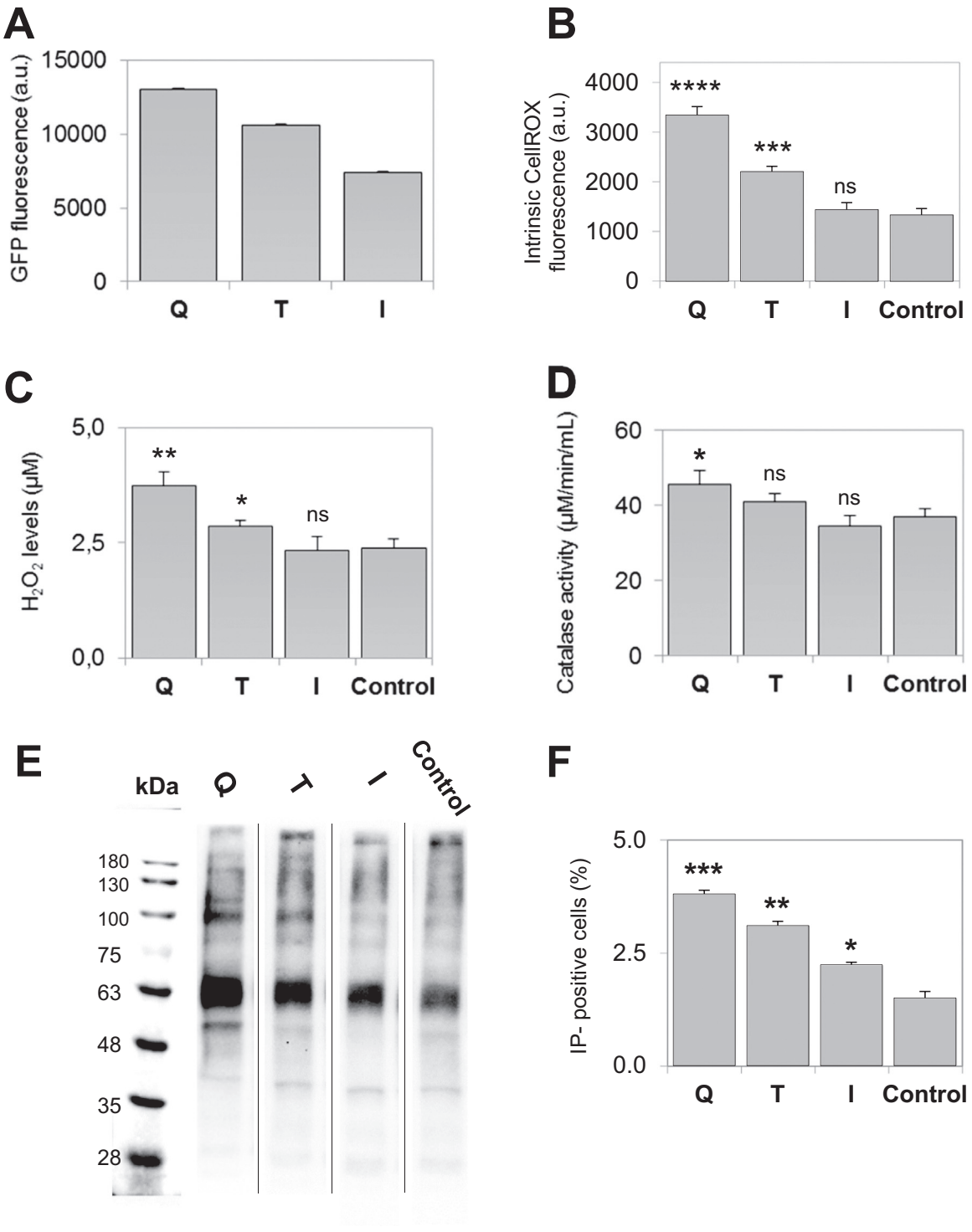

Fig. 2. Analysis of *S. cerevisiae* cultures expressing Gln, Thr and Ile mutants for 16 h. (A) Median fluorescence values of expressed GFP from 10,000 cells determined by FC analysis (FITC-A) for selected Aβ42-GFP variants. (B) CellROX median fluorescence intensity (APC-A) (as indicator of oxidative stress levels) determined by FC for selected Aβ42-GFP variants. Error bars represent CV of the FC gated cells (P3 population). (C) H_2O_2 levels determined by monitoring the fluorescence at 595 nm for selected Aβ42-GFP variants. Error bars represent ± SE (n = 3). (D) Catalase activity determined by absorbance measures at 550 nm for selected Aβ42-GFP variants. Error bars represent ± SE (n = 3). (E) Immunodetection of protein carbonylation levels of insoluble cell fractions for selected Aβ42-GFP variants. All samples were run in the same gel. The places where the membrane was trimmed are indicated by a thin line. The normalised densities of the bands are: 135, 124, 88 and 100 a.u. for variants ordered from left to right, respectively. (F) The percentage of IP positive cells (as indicator of cell mortality) was obtained by FC analysis (PerCP-Cy5-A) for selected variants. Error bars represent ± SE (n = 3). Cells expressing GFP alone were used as control.

PVDF membrane, the digested fractions were detected by western blotting as previously described.

2.12. Statistical analysis

Statistical significance was determined using the two-tail *t*-Test. P values < 0.05 were considered statistically significant.

3. Results

3.1. The Aβ42-GFP protein collection

In the present study we used a set of 20 Aβ42-GFP variants that correspond to all possible mutations for residue 19 in the Aβ42 peptide [32]. This residue is located in the central hydrophobic cluster (CHC) of the peptide and has an important influence in the peptide's folding, self-assembly and structure in the fibrillar state [46,47]. Predictions of the aggregation propensities of the resulting sequences using the AGGRESCAN algorithm [48] anticipated that this protein dataset would display a continuum of aggregation propensities (Fig. S1). Analysis with predictors based on different physicochemical and structural protein properties such as TANGO [43] and Foldamyloid [44] rendered very similar aggregation gradation, ascribing in all cases the highest aggregation propensities to the natural Aβ42 sequence (Phe19) and those variants in which this residue is substituted by other aromatic or aliphatic residues (Fig. S1).

3.2. PI formation propensity of Aβ42-GFP variants

The 20 Aβ–GFP proteins were expressed individually in yeast under the control of the galactose-inducible GAL1 promoter to allow a rapid, strong and synchronous induction of protein expression. All yeast cells exhibited fluorescence 16 h after induction of protein expression. However, the formation of PI was observed only for 10 out of the 20 assayed variants. Representative images of selected PI-forming and PI–non-forming variants are shown in Fig. 1A. The 10 PI-forming variants correspond precisely with those proteins displaying the highest aggregation propensity in the AGGRESCAN scale (Fig. 1B). This points to a defined protein aggregation propensity threshold governing the PI formation in *S. cerevisiae*. In the conditions of our assay, this limit corresponds to ~ 45% of the aggregation potential of wild type Aβ. Below this threshold, and independently of the considered mutant, none of the cells in the population forms PI, whereas above this value the proportion of cells displaying PI sharply depends on the identity of the mutant, varying from 10% for Thr to > 60% for the wild type or the Ile mutant. Then by focussing on the set of PI forming mutants, we observed that the fraction of cells containing PI and the predicted aggregation propensities according to AGGRESCAN significantly correlate ($r = 0.90$, $p \leq 0.0001$) (Fig. 1C). The slope of the regression line (0.85) indicates that, above the aggregation threshold, a 10% increase of protein aggregation propensity of the peptide results in an 8.5% increase of the proportion of cells displaying protein inclusions.

3.3. The oxidative stress induced by Aβ42-GFP variants has a negative correlation with their aggregation propensity

In order to decipher whether the formation of intracellular PI causes or protects from oxidative stress, we selected three different Aβ–GFP variants for further study: i) Ile as a representative of high PI formation, ii) Thr as a representative of low PI formation and iii) Gln as a variant that does not generate PI.

In Aβ–GFP fusions, the GFP fluorescence acts as a reporter of the aggregation propensity, in such a way that more fluorescence indicates less aggregation and *vice versa* [49]. In agreement with the proportion of PI forming cells, the median of the population fluorescence measured by flow cytometry (FC) indicates that Gln is the most fluorescent variant, Ile is the less fluorescent and Thr has a fluorescence intensity in between the other two (Fig. 2A).

Then we monitored the oxidative stress caused by the expression of these variants by measuring four different parameters: ROS production, H_2O_2 levels, catalase activity and protein carbonylation. To monitor the ROS production we analysed the cells expressing the three Aβ–GFP variants with CellROX fluorogenic probe and FC (Table S1). The Gln variant exhibited the highest levels of ROS, followed by Thr and Ile (Fig. 2B). Therefore, the more soluble variant (Gln) caused the highest level of oxidative stress and the most aggregation-prone mutant (Ile) turned out to be the most innocuous. These results were confirmed by the levels of H_2O_2 (Fig. 2C), again Gln exhibited the highest levels of oxidative stress and Ile the lowest, with Thr displaying intermediate H_2O_2 levels. In agreement, the enzyme catalase, which protects against ROS, showed higher activity in yeast strains expressing the Gln variant than in those expressing the Ile one (Fig. 2D). Protein carbonyl formation is a marker for protein oxidation and can be detected by DNPH derivatization followed by western blot with anti-DNP antibodies [50]. We fractioned yeast cells and analysed the level of carbonylation in both the soluble and insoluble protein fractions by western blot. Whereas we did not observe any significant differences between soluble fractions, the level of protein oxidation was clearly higher in the insoluble fraction of cells expressing the Gln variant than in those expressing the Ile one (Fig. 2E).

In order to assess whether the recorded levels of oxidative stress may impact cell fitness, we analysed the viability of cells expressing the different variants by FC using propidium iodide (IP) staining. IP is a DNA-binding dye that is excluded by live cells, but enters dead cells with damaged membranes. In good agreement with their relative ROS levels, the viability of the cell population was more compromised for the Gln variant than for Ile (Fig. 2F).

The above described results suggest that PI formation is not the main elicitor of cellular oxidative stress. To confirm this, we used confocal fluorescence microscopy and dihydroethidium fluorescence, a marker of intracellular oxidative stress, to detect whether the cellular distribution of Gln and Ile protein variants correspond with sites of ROS production. In good agreement with the above described data, the levels of ROS are higher in the more soluble Gln variant (Fig. 3). In both cases, the oxidative stress is distributed in the cytosol and does not co-localise with IP, suggesting that they are not centres of oxidative events as proposed by other studies [21].

To address the relationship between protein aggregation properties and oxidative stress in a more quantitative manner, we monitored the levels of ROS for the rest of mutants belonging to the Aβ–GFP collection using CellROX and FC (Table S1). Then, we compared the levels of ROS with the aggregation propensity predicted by three different algorithms (Fig. 4A, Fig. S3A and S3B) and with all of them we obtained a significant negative correlation (AGGRESCAN: $r = 0.91$, $p \leq 0.0001$; TANGO: $r = 0.82$, FoldAmyloid: $p \leq 0.0001$; $r = 0.84$, $p \leq 0.0001$).

The aggregation propensity of a polypeptide sequence in a defined environment depends on its physicochemical properties [51]. In this context, it has been found that β-sheet propensity and hydrophobicity favour the self-assembly of proteins into aggregates. Consistently, our results show that these two protein properties correlate negatively with oxidative stress levels (β-sheet propensity: $r = 0.72$, $p \leq 0.0001$, Fig. 4B; hydrophobicity: $r = 0.78$, $p \leq 0.0001$, Fig. 4C).

3.4. Both PI formation and aggregation-prone protein clearance prevent oxidative stress

The comparison between GFP fluorescence, an indication of aggregation, and the oxidative stress shows a significant positive relationship ($r = 0.68$, $p \leq 0.0001$) though the correlation coefficient is lower than the one observed for predicted aggregation propensities (Fig. 5A). In this distribution, Trp and Phe are clear outliers, essentially because they display lower fluorescence than expected. This matches with the

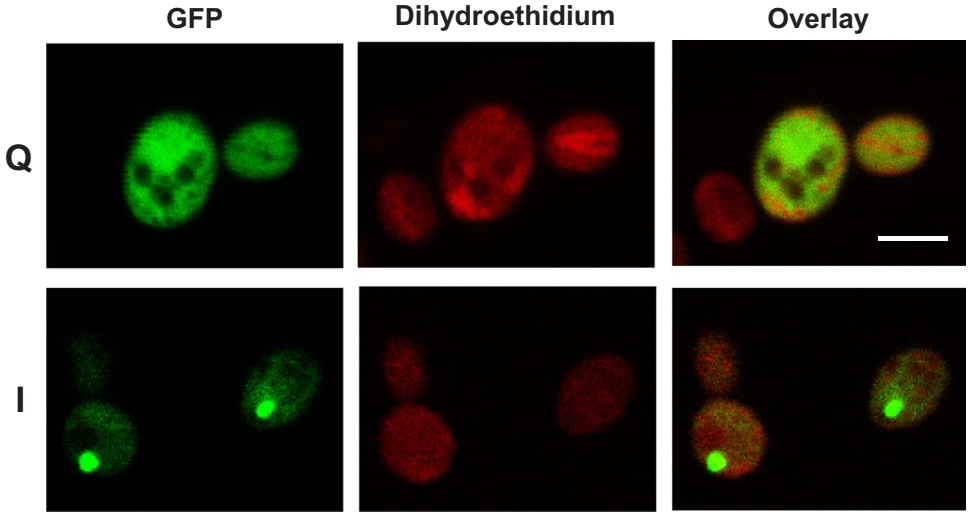

Fig. 3. Characterisation of GFP fluorescence and oxidative stress levels for Gln and Ile variant. Representative confocal microscopy images of yeast cells expressing Gln and Ile variants showing the levels of GFP fluorescence (left), cellular oxidative stress (middle) and overlay image (right). Induced cultures were incubated with 10 μM dihydroethidium prior to image acquisition. Scale bar represents 5 μm.

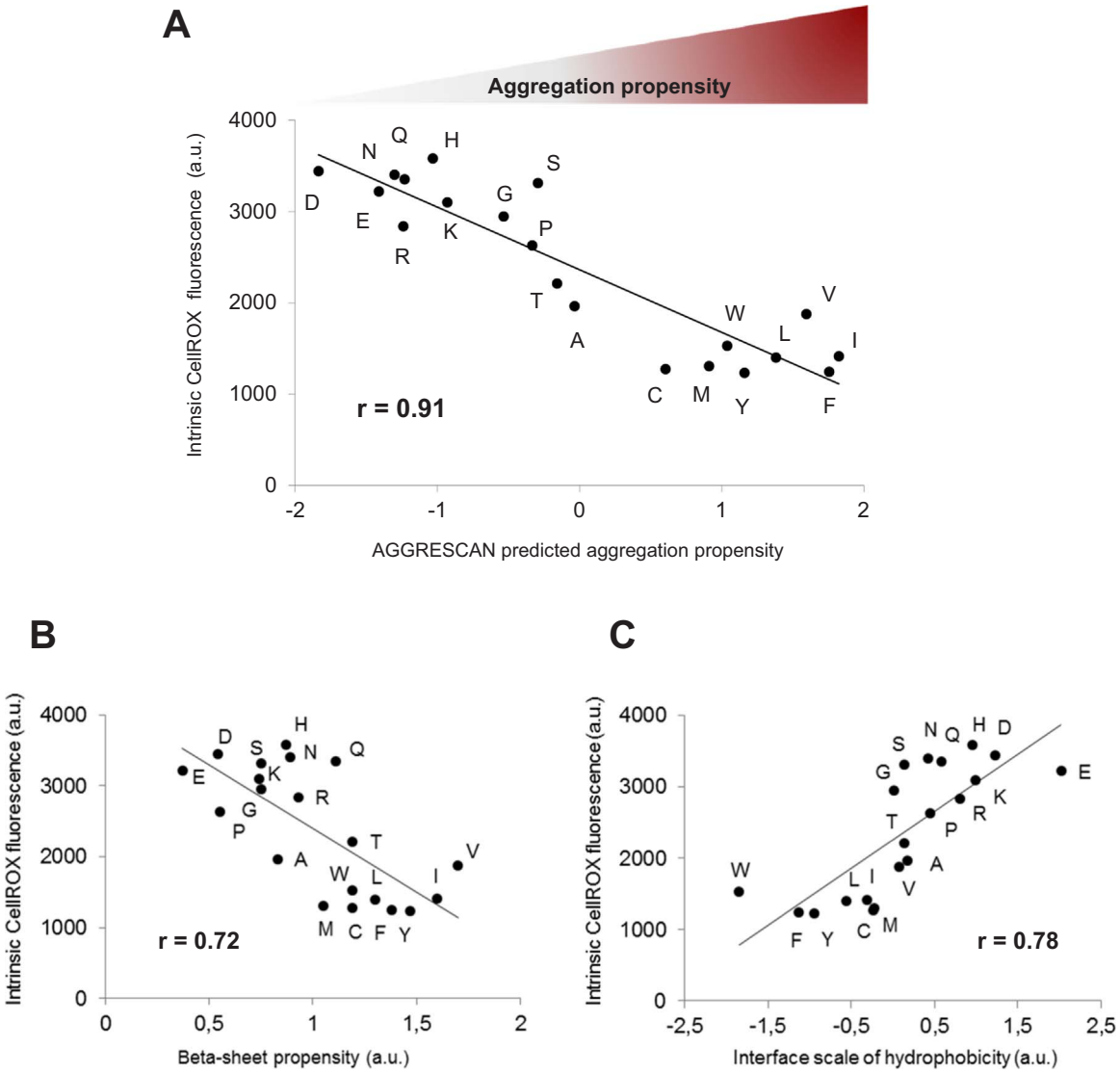

Fig. 4. Relationship between intrinsic oxidative stress levels of 20 Aβ42-GFP mutants with AGGRESCAN predicted aggregation propensities and amino acid physicochemical properties. Correlation between CellROX intrinsic fluorescence and: (A) intrinsic aggregation propensity predicted by AGGRESCAN ($r = 0.91$, $p \leq 0.0001$); (B) β-sheet propensity from Chou and Fasman scale ($r = 0.72$, $p \leq 0.0001$) and (C) hydrophobicity derived from the interface scale ($r = 0.78$, $p \leq 0.0001$).

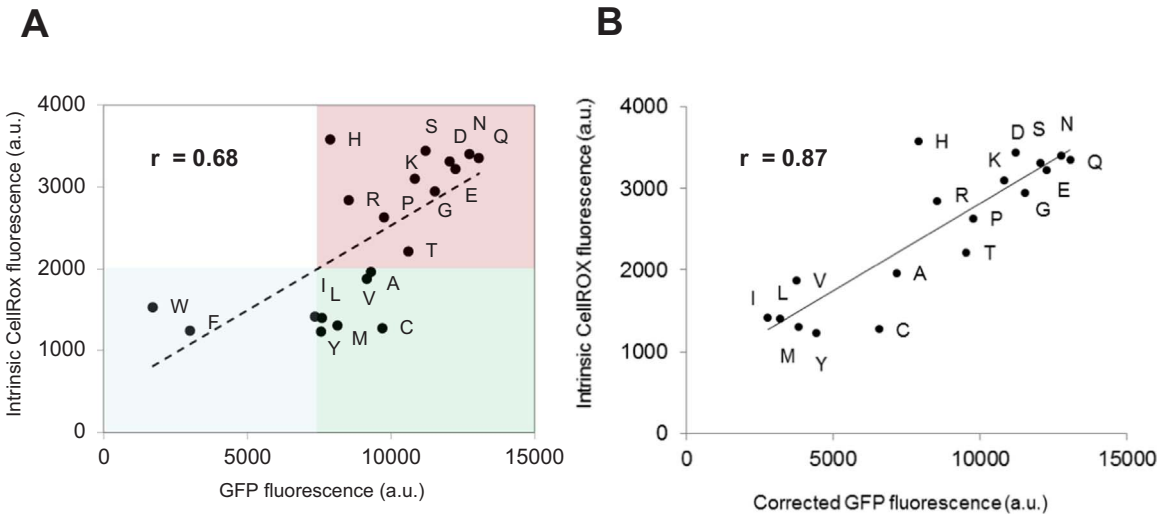

Fig. 5. Correlation between GFP fluorescence and intrinsic levels of oxidative stress of the expressed 20 mutants from Aβ42-GFP set. (A) Spatial distribution of Aβ42-GFP mutants depending on GFP fluorescence *vs*. intrinsic levels of oxidative stress is represented. In blue: mutants with low levels of oxidative stress presenting low levels of GFP fluorescence. In green: mutants with low levels of oxidative stress presenting high levels of GFP fluorescence. In red: mutants with high levels of oxidative stress presenting high levels of GFP fluorescence ($r = 0.68$, $p \leq 0.0001$). (B) Correlation between corrected GFP fluorescence, after removing the variants that behave as outliers from the dataset (Phe and Trp), and intrinsic levels of oxidative stress for mutants expressing Aβ42-GFP, ($r = 0.87$, $p \leq 0.0001$).

smaller and less fluorescent PI they exhibit, in comparison with the other aggregation-prone mutants (Fig. S4). In addition, we have previously shown that these observations are linked to the fact that Trp and Phe mutants are recognised by the protein quality machinery and degraded through autophagy [39], resulting in very low protein levels (Fig. 6A). All these observations suggest that the degradation of an aggregation-prone variant or sequestering it in PI may result in a similar prevention of oxidative stress.

However, Trp and Phe are not the only responsible for the observed lower correlation, since removing them from the dataset only increases the correlation coefficient to $r = 0.72$ ($p \leq 0.0001$). We must consider the observation that PI contribute much more to GFP fluorescence than they do to oxidative stress levels (Fig. 3). Thus, taking only into consideration the fluorescence of non-PI forming cells, the correlation coefficient raises to $r = 0.87$ ($p \leq 0.0001$; Fig. 5B), supporting that PI have a low impact on the generated oxidative stress levels.

3.5. Aggregated but diffusely distributed protein species are the elicitors of oxidative damage

To further study the link between cellular oxidative stress and the soluble/aggregated state of the Aβ42-GFP variants, we measured their distribution between the soluble and insoluble cell fractions using western blotting (Fig. 6A). Irrespective of whether the proteins can form PI, the 20 variants were found to be mainly located in the insoluble fraction, consistently with previous data obtained by our group and others [39,52]. However, the levels of soluble protein are higher for polar and charged residues compared to the hydrophobic ones (Fig. 6B).

The fact that mutants diffusely distributed in the cytosol displayed levels of insoluble protein equivalent or even higher than those forming PI was surprising (Fig. 6B). This argues that the insoluble fraction might contain at least two types of aggregates, one corresponding to PI and the other to proteins that, despite being aggregated, do not coalesce in visible inclusions, remaining homogenously distributed through the cytosol; we will call this last type diffuse aggregates.

With the aim to localize the protein species generating the oxidative stress, we analysed whether the measured CellROX fluorescence correlates with the detected protein levels in either the soluble or the insoluble fraction. The correlation with the levels of soluble fraction was higher than with the levels of insoluble fraction (Fig. 6C). From these results we discarded PI as centres of oxidative stress and considered two possible interpretations: (i) the soluble species themselves correspond to the reactive forms, or (ii) the diffuse aggregates are the reactive forms and the levels of soluble protein are just a reflection of the levels of these disseminated assemblies in the insoluble fraction. In order to discriminate between these two possibilities, we sought to design a novel Aβ42 variant with enhanced solubility, in such a way that the amount of protein in the soluble fraction would be higher than the amount in the insoluble one, while keeping sequence changes to a minimum. If the soluble species are the ROS promoting forms, we expected oxidative stress levels being higher in this mutant than in any other variant. Different aggregation prediction algorithms coincide to indicate that Aβ42 peptide consists of two main aggregation-prone stretches, comprising residues 17–21 and 30–41 (Fig. 7A). In the solid-state NMR, the structure of Aβ amyloid fibrils demonstrates that the residue Phe19 in the first β-strand interacts with Leu34 in the second β-strand [53]. Based on these data, we introduced in one of the most soluble and fluorescent variants (Aβ42-F19D) a second mutation by changing the original Leu at position 34 to Pro (a β-breaking residue), a combination (19Asp/34Leu) that we have already shown to be highly soluble in bacteria [54].

In good agreement with the design, 16 h after induction, cells expressing F19D/L34P variant exhibit a highly fluorescent cytosol devoid of any PI (Fig. 7B). Fractionation of cell content and immunoblotting indicated that, as intended, in 19Asp/34Leu the majority of the protein was now located in the soluble fraction (Fig. 7C). Quantitative analysis of the GFP fluorescence of cells expressing the double mutant using FC indicates that this mutant is by far the most fluorescent variant in the protein set (Fig. 7E). Despite these properties, the levels of protein carbonylation (Fig. 7D) and oxidative stress (Fig. 7F) that it induced were moderate, which discards the possibility of soluble species being the main elicitors of oxidative damage. To asses if this effect is caused instead by diffuse aggregates, we took profit of the kinetics of protein aggregation. Therefore, we expressed the double mutant for 48 h. At this time point, even if the fluorescence remains diffusely distributed in the cytosol (Fig. 7B), the large majority of the protein is now located in the insoluble fraction (Fig. 7C). Thus, in these conditions, the double mutant resembles Gln variant after 16 h of induction of protein expression. We also expressed Gln, Thr and Ile mutants for 48 h and monitored the distribution of GFP fluorescence in the cytosol at this time point (Fig. 8A). A proportion of Gln expressing

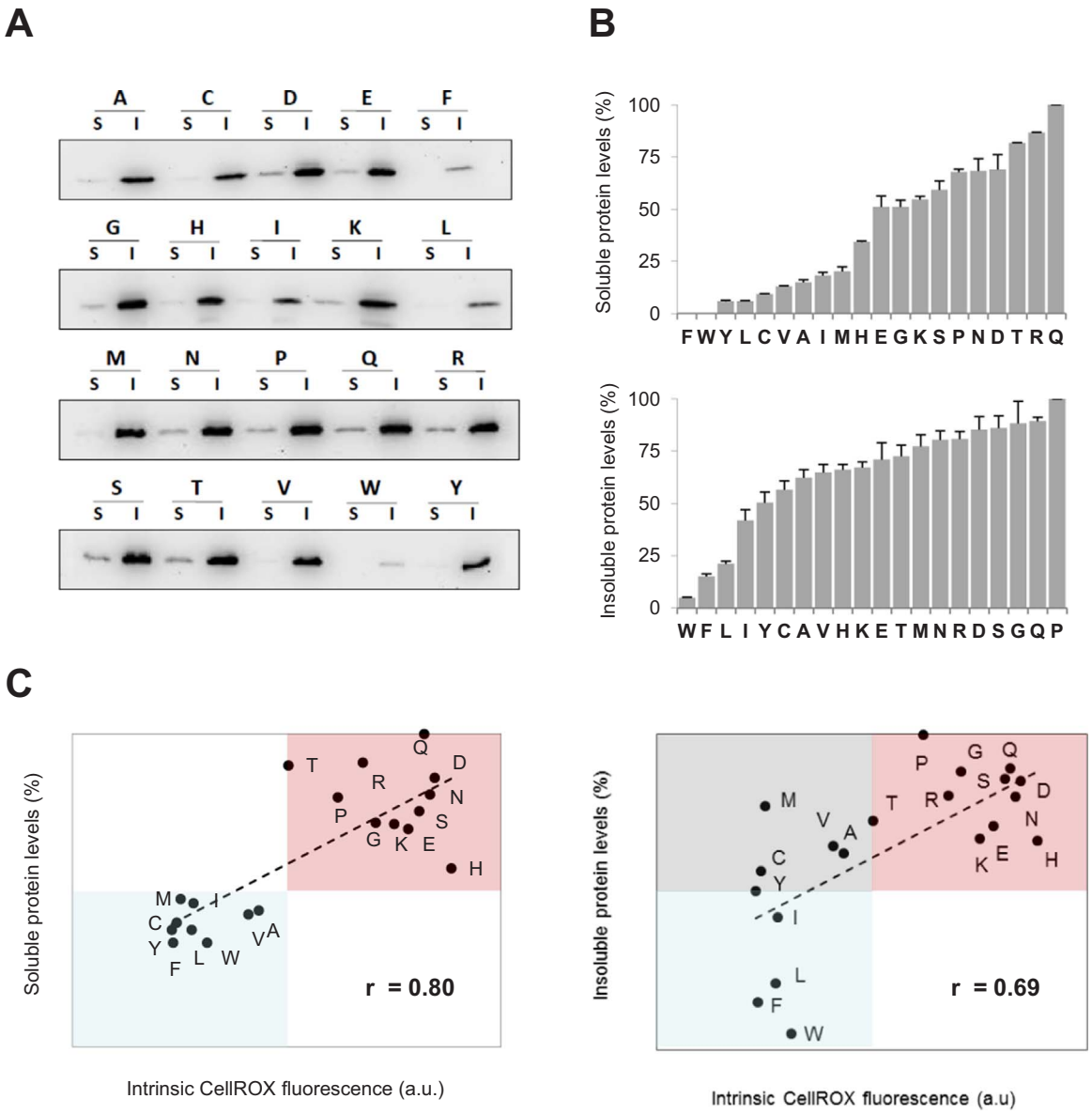

Fig. 6. Characterisation of 20 Aβ42-GFP mutants expression after 16 h. (A) Immunodetection of soluble (S) and insoluble (I) cell fractions of the 20 Aβ42-GFP variants. Detected bands correspond to MW =35 kDa. (B) Bar graph with the percentage values of the soluble and insoluble protein fractions quantified using Quantity One software. Error bars represent ± SE (n=3). (C) Relation between the intrinsic levels of oxidative stress *vs.* soluble and insoluble protein fractions of Aβ42-GFP variants. The spatial distribution of Aβ42-GFP mutants depending on CellROX intrinsic fluorescence and the corresponding protein levels: (blue) mutants with low levels of corresponding protein fraction of Aβ42-GFP displaying low oxidative stress levels; (red) mutants with high levels of corresponding protein fraction of Aβ42-GFP presenting high oxidative stress levels and; (grey) mutants with high levels of corresponding protein fraction of Aβ42-GFP showing low oxidative stress levels. Correlation index for soluble protein levels: r=0.80, p≤0.0001; for insoluble protein levels: r =0.69, p≤0.0001.

cells begin to display PI, the inclusions of Thr become similar to those of Ile at the 16 h, and in yeast cells expressing Ile variant all the fluorescence is concentrated in PI at 48 h. Comparison of the relative levels of oxidative stress for the four mutants at 16 h and 48 h time points, as determined by using FC (Fig. 8B), allows to visualise that the highest oxidative stress is attained when the protein is diffusely distributed in the cytosol but located in the insoluble fraction like in the case of Gln at 16 h or the double mutant at 48 h, whereas the formation of PI inclusions results in reduced levels of oxidative stress. After 48 h, cells expressing the double mutant display slightly lower viability than the other variants (Fig. 8C), whereas at 16 h it is the Gln variant that induces the highest mortality (Fig. 8C).

To further understand the properties of these diffuse aggregates we addressed whether they might display a compact structure by monitoring their accessibility to proteinase K (PK) (Fig. 8D). Despite its high activity for cleaving peptide bonds, PK cannot attack the highly packed backbones in an amyloid β-sheet structure. The insoluble fractions of cells expressing Ile, Thr, Gln and 19Asp/34Leu variants were treated with PK up to 10 min. Interestingly, at 16 h the aggregated fraction of Gln cells was essentially resistant to proteolysis. The same was true for the insoluble fraction of 19Asp/34Leu after 48 h, which indicates that diffusely distributed aggregates already possess an amyloid-like conformation able to elicit the oxidative stress response. The lower levels of insoluble Ile protein at 48 h suggest that this mutant resembles now Trp or Phe at the 16 h, becoming a substrate for active degradation.

The above observed influence of the aggregation kinetics on ROS promoted levels, predicts that at early times, when aggregation-prone mutants still haven't been compacted in large and localised inclusions, these variants would promote more oxidative stress and cytotoxicity than their more soluble counterparts. To validate this prediction, Gln and Ile mutants were analysed 8 h after induction of protein expression. At this time point, Gln fluorescence was homogenously distributed in the cytosol, whereas in the case of Ile, multiple small fluorescent foci were already observable in the cells (Fig. 9A). As expected, the levels of

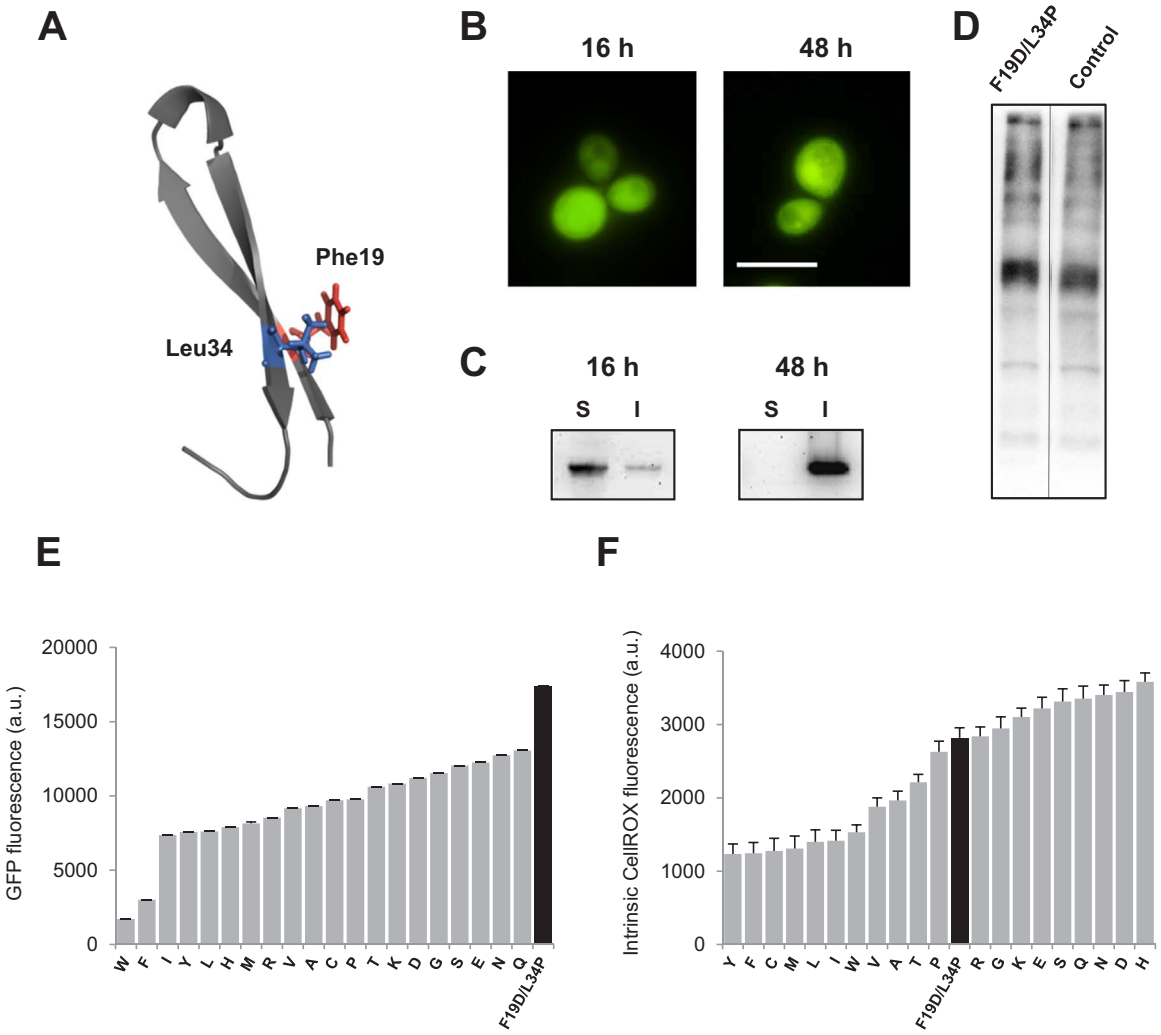

Fig. 7. Characterisation of Aβ42-F19D/L34P variant. (A) Structure of Aβ42 peptide (PDB: 2OTK) showing the side chains of double mutant, F19 in red and L34 in blue. (B) Representative fluorescence microscopy images of yeast cells expressing Aβ42-F19D/L34P-GFP variant for 16 and 48 h showing GFP fluorescence. Scale bar represents 10 μm. (C) Western blotting of the soluble (S) and insoluble (I) cell fractions of the mentioned variant after 16 and 48 h of expression. Detected bands correspond to MW ≈35 kDa. (D) Immunodetection of protein carbonylation levels of insoluble cell fractions for Aβ42-F19D/L34P and pESC-URA-GFP. The normalised densities of the bands are: 103 for Aβ42-F19D/L34P and 100 a.u. for pESC-URA-GFP. Both samples were run in the same gel. The place where the membrane was trimmed is indicated by a thin line. (E) Bar graph representing the median GFP fluorescence (FITC-A channel) of P2 population, for each expressed Aβ42-GFP variant, together with Aβ42-F19D/L34P, acquired by FC. (F) Bar graph representing median fluorescence intensity of CellROX probe (APC-A channel) (levels of oxidative stress) of P3 population determined by FC. Error bars represent CV of the FC gated cells.

GFP fluorescence, measured by FC, were higher in Gln expressing cells (Fig. 9B), but contrary to what was observed at 16 h, after 8 h of expression it is the more aggregation-prone Ile variant that exhibits the highest levels of oxidative stress (Fig. 9C) and the lowest viability (Fig. 9D).

4. Discussion

Many late-onset neurodegenerative diseases are linked to the presence of aggregation-prone proteins [1–5]. It has been observed that mutations causing or exacerbating these proteinopathies increase, in many cases, the protein propensity to form aggregates, thus linking the formation of protein deposits in the brain and the degeneration of the nervous system [55]. Also, there are mounting evidences for a major contribution of oxidative stress in the pathology of these disorders [56,57], with clear indications of oxidative damage to lipids, proteins and DNA in patient's post-mortem brains [19,24,26,27]. The connection between protein aggregation propensity and oxidative stress has been demonstrated in models of HD, where the aggregation tendency of the protein is determined by the length of the poly(Q) expansion, longer poly(Q) stretches being more aggregation-prone and inducing higher ROS production than shorter segments in wild type sequences [58]. However, a systematic quantitative investigation of the relationship between protein aggregation propensities and intracellular oxidative stress is still missing. In the present work, we addressed this issue, taking advantage of a set of 20 Aβ variants differing in a single residue, but displaying a continuous range of aggregation propensities when expressed in the yeast cytosol. The obtained data have allowed us to dissect the contribution of the different species populating the aggregation reaction to intracellular ROS production.

The different aggregation properties of the 20 Aβ42-GFP variants in the present study translate into a binary ability to form PI, half of the proteins forming visible aggregates and the rest remaining diffusely distributed in the cytosol. This illustrates the exquisite control that the sequence exerts on *in vivo* aggregation propensities, since these fusions differ in a single amino acid out of more than 300 residues. Indeed, above the PI formation threshold, there is a linear correlation between the aggregation propensity of a sequence and its recruitment into PI (Fig. 1C).

As for poly(Q) extensions [58], we expected that the oxidative insult would increase as the aggregation propensities of the expressed variants augmented. However, we found exactly the contrary, an almost perfect

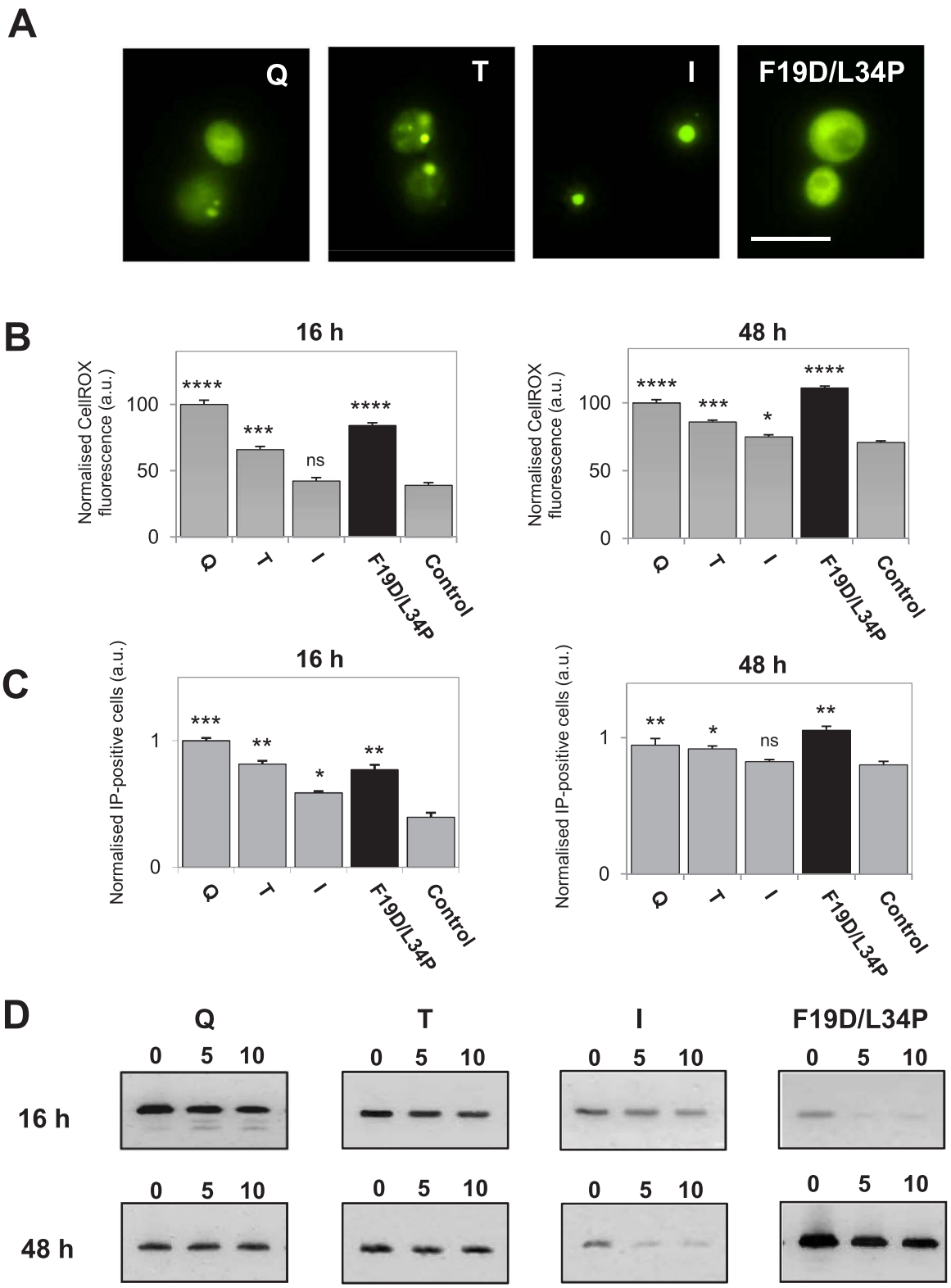

Fig. 8. Comparison between GFP fluorescence, oxidative stress levels, cell viability and proteinase K (PK) resistance for Aβ42-GFP mutants after 16 and 48 h of expression. (A) Representative fluorescence microscopy images showing GFP signal of yeast cells expressing selected Aβ42-GFP variants (Gln, Thr, Ile and F19D/L34P) for 48 h. Scale bar represents 10 μm. (B) CellROX median fluorescence bar graph of yeast cultures expressing selected Aβ42-GFP variants induced for 16 and 48 h determined by FC analysis. Error bars represent CV from 10,000 events. (C) Percentage of IP positive cells in cultures expressing selected Aβ42-GFP variants induced for indicated times. Error bars represent ± SE (n = 3). (D) Time-lapse PK resistance of insoluble fractions of selected Aβ42-GFP variants, induced for 16 and 48 h, detected by western blotting. Detected bands correspond to MW = 35 kDa. Cells expressing GFP alone were used as control.

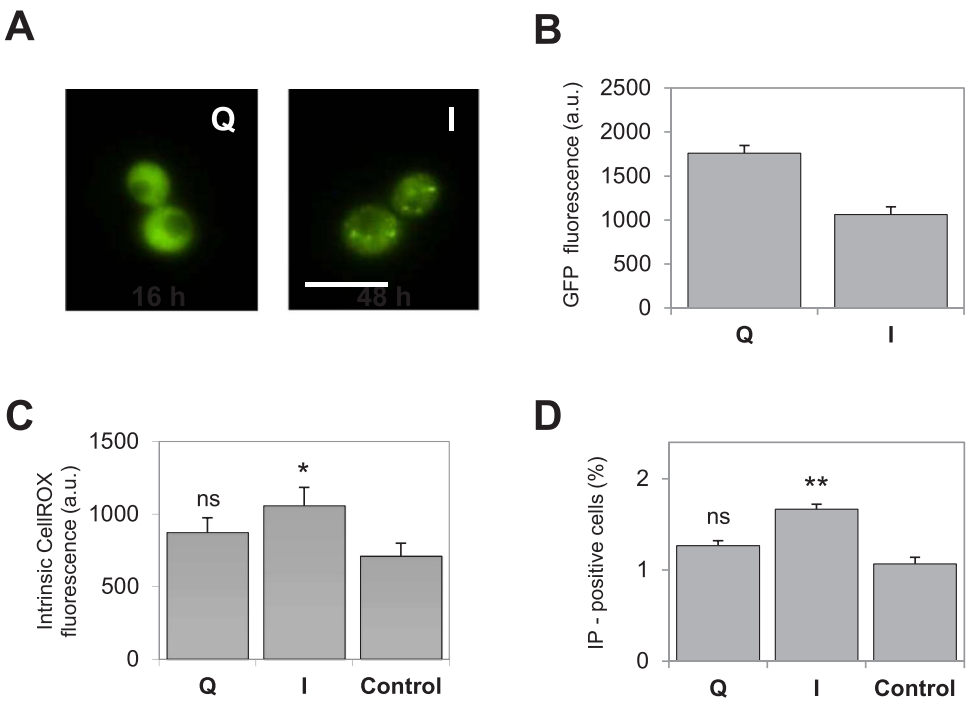

Fig. 9. Characterisation of GFP fluorescence, oxidative stress levels and cell viability for *S. cerevisiae* cultures expressing Gln and Ile Aβ42-GFP mutants for 8 h. (A) Representative fluorescence microscopy images of yeast cells expressing selected variants for 8 h. Scale bar represents 10 μm. (B) Median fluorescence values of expressed GFP from 10,000 cells determined by FC analysis (FITC-A) for selected Aβ42-GFP variants. (C) CellROX median fluorescence intensity (APC-A) (as indicator of oxidative stress levels) determined by FC in selected Aβ42-GFP variants. Error bars represent CV of the FC gated cells (P3 population). (D) The percentage of IP positive cells (as indicator of cell mortality) was obtained by FC analysis (PerCP-Cy5-A) for selected variants. Error bars represent ± SE (n = 3). Cells expressing GFP alone were used as control.

negative correlation (r = 0.91 and slope = 1) between the protein aggregation potential and the oxidative stress it elicits. Accordingly, the proteins in the set can be classified in two classes: I) variants with low aggregation propensity and high oxidative stress and II) mutants with high aggregation tendency and low oxidative potential. Cells expressing class I mutants produced significantly higher levels of hydrogen peroxide and contained significant higher catalase activity than class II variants, indicating that they suffer from a higher oxidative stress that activates the antioxidant defences. Expression of class I mutants also resulted in a higher level of insoluble carbonylated proteins and a lower viability. As a general trend, in the first class we find polar and charged residues with low β-sheet propensity in position 19 of Aβ42, whereas in the second one we find hydrophobic residues with higher β-sheet tendency. Again, this observation was counterintuitive, since in aggregation-prone proteins more hydrophobic variants are usually associated with disease early onset [59]. Importantly, variants in the first class do not form observable PI, in contrast to those in the second class, which discards PI as the elicitors of oxidative damage (Fig. 1). Confocal microscopy clearly shows that PI do not produce significant levels of ROS (Fig. 3) and, indeed, it appears that sequestering the most aggregation-prone variants in PI is as effective to abrogate oxidative stress as their active degradation by the proteostasis machinery (Fig. 5).

The binary ability of Aβ42-GFP variants to form/not form PI, together with the lack of oxidant activity of these macromolecular assemblies, indicated that the diffusely distributed protein should include the reactive species. Contrary to what it was expected, it turned out that even in the less aggregation-prone mutants, in which PI were never observed, a large majority of the protein was located in the insoluble cell fraction. This reveals that, at least for our model, most of the protein homogeneously distributed through the cytosol is insoluble and correspond to what we call diffuse aggregates. Moreover, from this observation it becomes evident that inclusions and aggregates are not interchangeable terms. Engineering a highly soluble 19Asp/34Leu Aβ42-GFP variant we could discard the soluble, likely monomeric protein, as a significant source of ROS and assign this property to the diffuse aggregates. It is likely that, according to their aggregated and protease resistant nature, these species correspond to oligomeric and/or protofibrillar assemblies [20]. Our data are consistent with *in vitro* assays on Aβ40 showing that maximum production of free radicals occurs early in the aggregation reaction, where these small assemblies are maximally populated [60]. This will explain why the Ile variant is more toxic than Gln early after induction of protein expression (8 h) (Fig. 9), but this relationship is inverted at longer times (Figs. 2 and 8). Comparative analysis of the distribution, solubility and oxidative stress for different Aβ42-GFP variants at 16 and 48 h, suggest that when the protein aggregates are immobilized in intracellular PI, they are less dangerous, in agreement with the observation that *in vitro* formed Aβ40 mature fibrils exhibit a negligible oxidative potential [60]. Therefore, oxidative stress can be predicted just by monitoring the levels of diffuse, but aggregated species at a certain time point.

In folded proteins, hydrophobic residues are buried inside the core and their exposure is taken by the cell as an indicative of misfolding and is sufficient to target proteins to inclusion bodies [61]. We have observed that, due to its composition and short length, the intracellular expression of Aβ42 mimics the conditions of a misfolded conformer. The central hydrophobic cluster of Aβ42 includes residues 17–21 (LVFFA), thus the placement of a polar or charged residue in the central 19 position might disrupt this stretch and abrogate the misfolding recreation. This will explain why all the variants displaying hydrophobic mutations were recruited into PI whereas the most of the charged and polar ones were not [62]. This effect has been observed *in vivo* for the Aβ Arctic mutation (E22G), in which the removal of a flanking charge results in an enhanced formation of large PI, a reduction of the oligomer levels and decrease of the functional deficits in a transgenic mice model [63].

Our data provide evidence for a causal link between the accumulation of diffuse aggregates and cellular oxidative stress and suggest that PI formation acts as a second line protective strategy against the intracellular oxidative stress caused by these species. These findings are consistent with previous data with poly(Q)-expanded huntingtin

[64], ataxin-1 [65], androgen receptor [66] and α-synuclein [67], demonstrating a dissociation between PI formation and cell death. Our results have important implications for the therapeutics of the neurodegenerative disorders linked to protein aggregation. Approaches intended to prevent the formation of PI in the brain can convert a locally recruited inert protein into a toxic aggregated molecule disseminated around the cell, prolonging oxidative stress and the associated neurotoxicity. This is consistent with the observation that pharmacological or genetic disruption of the physiologic processes required for PI formation results in increased proteotoxicity [21,67]. On the other way around, reducing the lifetime of protein aggregates and/or promoting their sequestration into PI appear as worth to explore therapeutic strategies for the treatment of protein aggregation associated diseases [68].

Conflict of interest

The authors declare that they have no competing interests.

Acknowledgements

We thank Cristina Visentin for help with H_2O_2 and catalase measurements. This work was funded by the Spanish Ministry of Economy and Competitiveness (BFU2013-44763-P and BIO2016-783-78310-R to S.V.). S.V. has been granted an ICREA ACADEMIA award.

Appendix A. Supplementary material

Supplementary data associated with this article can be found in the online version at http://dx.doi.org/10.1016/j.redox.2017.03.027.

References

[1] C.M. Dobson, Getting out of shape, Nature 418 (2002) 729–730.
[2] F. Chiti, C.M. Dobson, Protein misfolding, functional amyloid, and human disease, Annu. Rev. Biochem. 75 (2006) 333–366.
[3] X. Fernàndez-Busquets, N.S. de Groot, D. Fernandez, S. Ventura, Recent structural and computational insights into conformational diseases, Curr. Med. Chem. 15 (2008) 1336–1349.
[4] A. Aguzzi, T. O'Connor, Protein aggregation diseases: pathogenicity and therapeutic perspectives, Nat. Rev. Drug Discov. 9 (2010) 237–248.
[5] M. Renner, R. Melki, Protein aggregation and prionopathies, Pathol. Biol. 62 (2014) 162–168.
[6] O.D. King, A.D. Gitler, J. Shorter, The tip of the iceberg: rna-binding proteins with prion-like domains in neurodegenerative disease, Brain Res. 1462 (2012) 61–80.
[7] D.M. Mitrea, R.W. Kriwacki, Phase separation in biology; functional organization of a higher order, Cell Commun. Signal. 14 (2016) 1.
[8] A.A. Hyman, C.A. Weber, F. Jülicher, Liquid-liquid phase separation in biology, Annu. Rev. Cell Dev. Biol. 30 (2014) 39–58.
[9] J. Frydman, Folding of newly translated proteins in vivo: the role of molecular chaperones, Annu. Rev. Biochem. 70 (2001) 603–647.
[10] M.H. Glickman, A. Ciechanover, The ubiquitin-proteasome proteolytic pathway: destruction for the sake of construction, Physiol. Rev. 82 (2002) 373–428.
[11] K.J. Travers, C.K. Patil, L. Wodicka, D.J. Lockhart, J.S. Weissman, P. Walter, Functional and genomic analyses reveal an essential coordination between the unfolded protein response and ER-associated degradation, Cell 101 (2000) 249–258.
[12] M.B. Metzger, S. Michaelis, Analysis of quality control substrates in distinct cellular compartments reveals a unique role for Rpn4p in tolerating misfolded membrane proteins, Mol. Biol. Cell. 20 (2009) 1006–1019.
[13] F.U. Hartl, A. Bracher, M. Hayer-Hartl, Molecular chaperones in protein folding and proteostasis, Nature 475 (2011) 324–332.
[14] E. Wong, E. Bejarano, M. Rakshit, K. Lee, H.H. Hanson, N. Zaarur, et al., Molecular determinants of selective clearance of protein inclusions by autophagy, Nat. Commun. 3 (2012) 1240.
[15] C.A. Ross, C.M. Pickart, The ubiquitin-proteasome pathway in Parkinson's disease and other neurodegenerative diseases, Trends Cell Biol. 14 (2004) 703–711.
[16] M. Arrasate, S. Mitra, E.S. Schweitzer, M.R. Segal, S. Finkbeiner, Inclusion body formation reduces levels of mutant huntingtin and the risk of neuronal death, Nature 431 (2004) 805–810.
[17] C.A. Ross, M.A. Poirier, Opinion: what is the role of protein aggregation in neurodegeneration? Nat. Rev. Mol. Cell Biol. 6 (2005) 891–898.
[18] E. Evangelisti, R. Cascella, M. Becatti, G. Marrazza, C.M. Dobson, F. Chiti, et al., Binding affinity of amyloid oligomers to cellular membranes is a generic indicator of cellular dysfunction in protein misfolding diseases, Sci. Rep. 6 (2016) 32721.
[19] G. Forloni, V. Artuso, P. La Vitola, C. Balducci, Oligomeropathies and pathogenesis of Alzheimer and Parkinson's diseases, Mov. Disord. 31 (2016) 771–781.
[20] E. Deas, N. Cremades, P.R. Angelova, M.H.R. Ludtmann, Z. Yao, S. Chen, et al., Alpha-synuclein oligomers interact with metal ions to induce oxidative stress and neuronal death in Parkinson's disease, Antioxid. Redox Signal. 24 (2016) 376–391.
[21] E. Cohen, J. Bieschke, R.M. Perciavalle, J.W. Kelly, A. Dillin, Opposing activities protect against age-onset proteotoxicity, Science 313 (2006) 1604–1610.
[22] A. Sydow, A. Van der Jeugd, F. Zheng, T. Ahmed, D. Balschun, O. Petrova, et al., Tau-induced defects in synaptic plasticity, learning, and memory are reversible in transgenic mice after switching off the toxic Tau mutant, J. Neurosci. 31 (2011) 2511–2525.
[23] F. Facchinetti, V.L. Dawson, T.M. Dawson, Free radicals as mediators of neuronal injury, Cell. Mol. Neurobiol. 18 (1998) 667–682.
[24] N.S. de Groot, M.T. Burgas, Is membrane homeostasis the missing link between inflammation and neurodegenerative diseases? Cell. Mol. Life Sci. 72 (2015) 4795–4805.
[25] X. Wang, W. Wang, L. Li, G. Perry, H. Lee, X. Zhu, Oxidative stress and mitochondrial dysfunction in Alzheimer's disease, Biochim. Biophys. Acta 2014 (1842) 1240–1247.
[26] D. Toulorge, A.H.V. Schapira, R. Hajj, Molecular changes in the postmortem parkinsonian brain, J. Neurochem. (2016) 27–58.
[27] M.A. Ansari, S.W. Scheff, Oxidative stress in the progression of Alzheimer disease in the frontal cortex, J. Neuropathol. Exp. Neurol. 69 (2010) 155–167.
[28] B.J. Tabner, O.M.A. El-Agnaf, M.J. German, N.J. Fullwood, D. Allsop, Protein aggregation, metals and oxidative stress in neurodegenerative diseases, Biochem. Soc. Trans. 33 (2005) 1082–1086.
[29] W.J.J. Firdaus, A. Wyttenbach, P. Giuliano, C. Kretz-Remy, R.W. Currie, A.-P. Arrigo, Huntingtin inclusion bodies are iron-dependent centers of oxidative events, FEBS J. 273 (2006) 5428–5441.
[30] V. Khurana, S. Lindquist, Modelling neurodegeneration in Saccharomyces cerevisiae: why cook with baker's yeast? Nat. Rev. Neurosci. 11 (2010) 436–449.
[31] S. Tenreiro, T.F. Outeiro, Simple is good: yeast models of neurodegeneration, FEMS Yeast Res. 10 (2010) 970–979.
[32] S. Treusch, S. Hamamichi, J.L. Goodman, K.E.S. Matlack, C.Y. Chung, V. Baru, et al., Functional links between Aβ toxicity, endocytic trafficking, and Alzheimer's disease risk factors in yeast, Science 334 (2011) 1241–1245.
[33] F. D'Angelo, H. Vignaud, J. Di Martino, B. Salin, A. Devin, C. Cullin, et al., A yeast model for amyloid-β aggregation exemplifies the role of membrane trafficking and PICALM in cytotoxicity, Dis. Model. Mech. 6 (2013) 206–216.
[34] A.A. Cooper, A.D. Gitler, A. Cashikar, C.M. Haynes, K.J. Hill, B. Bhullar, et al., Alpha-synuclein blocks ER-Golgi traffic and Rab1 rescues neuron loss in Parkinson's models, Science 313 (2006) 324–328.
[35] T.F. Outeiro, S. Lindquist, Yeast cells provide insight into alpha-synuclein biology and pathobiology, Science 302 (2003) 1772–1775.
[36] S. Krobitsch, S. Lindquist, Aggregation of huntingtin in yeast varies with the length of the polyglutamine expansion and the expression of chaperone proteins, Proc. Natl. Acad. Sci. USA 97 (2000) 1589–1594.
[37] S. Willingham, T.F. Outeiro, M.J. DeVit, S.L. Lindquist, P.J. Muchowski, Yeast genes that enhance the toxicity of a mutant huntingtin fragment or alpha-synuclein, Science 302 (2003) 1769–1772.
[38] S. Tenreiro, M.C. Munder, S. Alberti, T.F. Outeiro, Harnessing the power of yeast to unravel the molecular basis of neurodegeneration, J. Neurochem. 127 (2013) 438–452.
[39] A. Villar-Piqué, S. Ventura, Protein aggregation propensity is a crucial determinant of intracellular inclusion formation and quality control degradation, Biochim. Biophys. Acta 2013 (1833) 2714–2724.
[40] N. Sanchez de Groot, R.A. Gomes, A. Villar-Pique, M.M. Babu, A.V. Coelho, S. Ventura, Proteome response at the edge of protein aggregation, Open Biol. 5 (2015) 140221.
[41] M. Morell, N.S. de Groot, J. Vendrell, F.X. Avilés, S. Ventura, Linking amyloid protein aggregation and yeast survival, Mol. Biosyst. 7 (2011) 1121–1128.
[42] O. Conchillo-Solé, N.S. de Groot, F.X. Avilés, J. Vendrell, X. Daura, S. Ventura, AGGRESCAN: a server for the prediction and evaluation of "hot spots" of aggregation in polypeptides, BMC Bioinform. 8 (2007) 65.
[43] A.-M. Fernandez-Escamilla, F. Rousseau, J. Schymkowitz, L. Serrano, Prediction of sequence-dependent and mutational effects on the aggregation of peptides and proteins, Nat. Biotechnol. 22 (2004) 1302–1306.
[44] S.O. Garbuzynskiy, M.Y. Lobanov, O.V. Galzitskaya, FoldAmyloid: a method of prediction of amyloidogenic regions from protein sequence, Bioinformatics 26 (2010) 326–332.
[45] R.L. Levine, J.A. Williams, E.R. Stadtman, E. Shacter, Methods Enzymol. 233 (1994) 346–357.
[46] G. Bitan, S.S. Vollers, D.B. Teplow, Elucidation of primary structure elements controlling early amyloid beta-protein oligomerization, J. Biol. Chem. 278 (2003) 34882–34889.
[47] A. Morimoto, K. Irie, K. Murakami, Y. Masuda, H. Ohigashi, M. Nagao, et al., Analysis of the secondary structure of beta-amyloid (Abeta42) fibrils by systematic proline replacement, J. Biol. Chem. 279 (2004) 52781–52788.
[48] N.S. de Groot, V. Castillo, R. Graña-Montes, S. Ventura, AGGRESCAN: method, application, and perspectives for drug design, Methods Mol. Biol. 819 (2012) 199–220.
[49] N.S. de Groot, F.X. Aviles, J. Vendrell, S. Ventura, Mutagenesis of the central hydrophobic cluster in Abeta42 Alzheimer's peptide. Side-chain properties correlate with aggregation propensities, FEBS J. 273 (2006) 658–668.
[50] M.A. Sorolla, C. Nierga, M.J. Rodríguez-Colman, G. Reverter-Branchat, A. Arenas, J. Tamarit, et al., Sir2 is induced by oxidative stress in a yeast model of Huntington

disease and its activation reduces protein aggregation, Arch. Biochem. Biophys. 510 (2011) 27–34.
[51] F. Chiti, M. Stefani, N. Taddei, G. Ramponi, C.M. Dobson, Rationalization of the effects of mutations on peptide and protein aggregation rates, Nature 424 (2003) 805–808.
[52] P.R. Bharadwaj, G. Verdile, R.K. Barr, V. Gupta, J.W. Steele, M.L. Lachenmayer, et al., Latrepirdine (dimebon) enhances autophagy and reduces intracellular GFP-Aβ42 levels in yeast, J. Alzheimers Dis. 32 (2012) 949–967.
[53] T. Lührs, C. Ritter, M. Adrian, D. Riek-Loher, B. Bohrmann, H. Döbeli, et al., 3D structure of Alzheimer's amyloid-beta(1-42) fibrils, Proc. Natl. Acad. Sci. USA 102 (2005) 17342–17347.
[54] S. Navarro, A. Villar-Piqué, S. Ventura, Selection against toxic aggregation-prone protein sequences in bacteria, Biochim. Biophys. Acta - Mol. Cell Res. 1843 (2014) 866–874.
[55] G. Invernizzi, E. Papaleo, R. Sabate, S. Ventura, Protein aggregation: mechanisms and functional consequences, Int. J. Biochem. Cell Biol. 44 (2012) 1541–1554.
[56] K.J. Barnham, C.L. Masters, A.I. Bush, Neurodegenerative diseases and oxidative stress, Nat. Rev. Drug Discov. 3 (2004) 205–214.
[57] E. Niedzielska, I. Smaga, M. Gawlik, A. Moniczewski, P. Stankowicz, J. Pera, et al., Oxidative stress in neurodegenerative diseases, Mol. Neurobiol. 53 (2016) 4094–4125.
[58] S. Hands, M.U. Sajjad, M.J. Newton, A. Wyttenbach, In vitro and in vivo aggregation of a fragment of huntingtin protein directly causes free radical production, J. Biol. Chem. 286 (2011) 44512–44520.
[59] M. Stefani, Protein misfolding and aggregation: new examples in medicine and biology of the dark side of the protein world, Biochim. Biophys. Acta 2004 (1739) 5–25.
[60] B.J. Tabner, O.M.A. El-Agnaf, S. Turnbull, M.J. German, K.E. Paleologou, Y. Hayashi, et al., Hydrogen peroxide is generated during the very early stages of aggregation of the amyloid peptides implicated in Alzheimer disease and familial British dementia, J. Biol. Chem. 280 (2005) 35789–35792.
[61] T.K. Neklesa, C.M. Crews, Chemical biology: greasy tags for protein removal, Nature 487 (2012) 308–309.
[62] K. Bersuker, M. Brandeis, R.R. Kopito, Protein misfolding specifies recruitment to cytoplasmic inclusion bodies, J. Cell Biol. 213 (2016) 229–241.
[63] I.H. Cheng, K. Scearce-Levie, J. Legleiter, J.J. Palop, H. Gerstein, N. Bien-Ly, et al., Accelerating amyloid-beta fibrillization reduces oligomer levels and functional deficits in Alzheimer disease mouse models, J. Biol. Chem. 282 (2007) 23818–23828.
[64] F. Saudou, S. Finkbeiner, D. Devys, M.E. Greenberg, Huntingtin acts in the nucleus to induce apoptosis but death does not correlate with the formation of intranuclear inclusions, Cell 95 (1998) 55–66.
[65] I.A. Klement, P.J. Skinner, M.D. Kaytor, H. Yi, S.M. Hersch, H.B. Clark, et al., Ataxin-1 nuclear localization and aggregation: role in polyglutamine-induced disease in SCA1 transgenic mice, Cell 95 (1998) 41–53.
[66] J.P. Taylor, F. Tanaka, J. Robitschek, C.M. Sandoval, A. Taye, S. Markovic-Plese, et al., Aggresomes protect cells by enhancing the degradation of toxic polyglutamine-containing protein, Hum. Mol. Genet. 12 (2003) 749–757.
[67] M. Tanaka, Y.M. Kim, G. Lee, E. Junn, T. Iwatsubo, M.M. Mouradian, Aggresomes formed by alpha-synuclein and synphilin-1 are cytoprotective, J. Biol. Chem. 279 (2004) 4625–4631.
[68] R.A. Bodner, T.F. Outeiro, S. Altmann, M.M. Maxwell, S.H. Cho, B.T. Hyman, et al., Pharmacological promotion of inclusion formation: a therapeutic approach for Huntington's and Parkinson's diseases, Proc. Natl. Acad. Sci. USA 103 (2006) 4246–4251.